Bikorimana *et al.*
Stem Cell Research & Therapy (2025) 16:369
https://doi.org/10.1186/s13287-025-04465-5

Stem Cell Research & Therapy

RESEARCH

Open Access

ARM-X: an adaptable mesenchymal stromal cell-based vaccination platform suitable for solid tumors

Jean Pierre Bikorimana[1], Nehme El-Hachem[2], Gabrielle A. Mandl[1], Daniela Stanga[3], Jamilah Abusarah[4], Roudy Farah[1], Marina P. Gonçalves[3], Perla Matar[1], Malak Lahrichi[5], Sebastien Talbot[6] and Moutih Rafei[1,4,5*]

Abstract

Background In addition to triggering endosomal escape, the Accum® platform was recently reported for its ability to instill antigen cross-presentation properties in mesenchymal stromal cells (MSCs). Despite the promising results obtained with the first-generation vaccine using the A1 Accum® derivative (ARM vaccine), large quantities of cancer antigens were required to achieve meaningful therapeutic effects. Given this limitation, additional Accum® variants were engineered and tested for their ability to lower the need for large antigen quantities. A leading variant, AccuTOX®, was selected for that purpose.

Methods Several functional studies, including a series of antigen cross-presentation assays, were conducted using the SIIN-FEKL-specific T-cell clone B3Z. Analysis of endosomal escape and the effect of various anti-oxidant compounds were used to decipher the AccuTOX® mode of action in MSCs. The potency of the AccuTOX®-reprogramed MSCs (ARM-X) cells was evaluated in the context of therapeutic vaccination using immunocompetent C57BL/6 mice with three different pre-established solid tumor models. Various depletion studies were also conducted in animals to identify effector cells involved in the therapeutic response mediated by the ARM-X cells. Finally, the effect observed on murine ARM-X cells was validated on human MSCs along with an immunopeptidome study reflecting the cross-presentation potency of these reprogrammed human cells.

Results AccuTOX® can indeed trigger MSCs to cross-present antigens, even if pulsed with low doses of tumor antigens while retaining most of the innate properties of A1, including increased antigen uptake and processing, production of reactive oxygen species, endosomal escape and induction of the unfolded protein response (UPR). When tested against melanoma, pancreatic and colon cancer, therapeutic administration of the ARM-X vaccine, in combination with anti-PD-1, impairs tumor growth. Mechanistically, the ARM-X vaccine relies on efferocytosis by endogenous phagocytes and requires both $CD4^+$ and $CD8^+$ T cells, as their depletion leads to a loss in therapeutic function.

Conclusion Altogether, this second-generation ARM-X vaccine represents a platform adaptable to multiple solid tumors. In addition, our data clearly allude to a direct link between AccuTOX®-mediated UPR activation and antigen cross-presentation by MSCs. The fact that these modulated MSCs become antigen-presenting cells via UPR stimulation opens-up a new line of investigation to search for additional agents capable of specifically activating this pathway to convert culture-adapted MSCs to a cellular vaccination tool adaptable to various cancer indications.

Keywords Allogeneic cell vaccine, AccuTOX®, Mesenchymal stromal cells, Endosomal escape, Antigen cross-presentation, Reactive oxygen species, Unfolded protein response, Immunopeptidome

*Correspondence:
Moutih Rafei
moutih.rafei.1@umontreal.ca
Full list of author information is available at the end of the article

Introduction

According to World Health Organization reports, cancer remains a global threat with over 10 million deaths annually [1]. These numbers attest to a dire need not only for better treatment options, but for effective protective measures against cancer development, as well. Furthermore, cancer recurrence or relapse after remission remain critical concerns, further highlighting the importance of developing suitable protective treatment strategies [2–4]. Among the major advancements being introduced in the field of immunotherapy, cancer vaccines are uniquely important, as their ultimate goal is to educate the immune system to generate effective anti-tumoral responses, ideally with long-term memory [4–8]. So far, Sipuleucel-T is the only FDA-approved dendritic cell (DC) cancer vaccine, targeting prostate cancer via the prostatic acid phosphatase (PAP) antigen presented on patients' DCs [9–11]. Although it was long believed that the administration of ex vivo developed DCs could bypass hurdles related to antigen delivery in vivo, Sipuleucel-T remained weak in stimulating potent and long-lasting immunity, resulting in poor clinical outcomes [12, 13].

Focusing on new means to stimulate antigen cross-presentation for mounting meaningful immune responses led to the introduction of mesenchymal stromal cells (MSCs) as a possible vaccination platform to overcome the main hurdles reported with DC vaccines [14–17]. While the use of MSCs in the clinic is generally favored for the convenience of their accessibility, flexibility, and the ease of culturing, and expanding them in vitro [18–22], most of the clinical roles of MSCs focuses on their well-studied regenerative and immunosuppressive properties [21–26]. However, increased research on the pro-inflammatory properties of MSCs under specific conditions opened the door for a new role in the field of vaccination using different modalities [14–17, 27–33]. Specifically, reprogramming of MSCs into potent antigen presenting cells (APCs) was recently achieved using various genetic engineering strategies or pharmacological conditioning [14, 16, 17, 32, 34, 35]. Interestingly, reprogrammed MSCs underwent several changes in gene expression and/or molecular levels and behaved as effective APCs exhibiting the ability to capture, process and cross-present exogenous antigens through major histocompatibility complex (MHC) class I molecules to $CD8^+$ T cells, leading to effective targeted immune responses [14, 17, 35]. Interestingly, additional data shared from recent studies in the field of cancer therapy reveal unique properties of MSCs such as their capacity to home to tumor sites, to modulate the tumor microenvironment by recruiting immune cells, and to potentiate anti-tumor effects in combination with other cancer treatment strategies [36–39]. Altogether, the data available on MSCs, further support the potential utility of reprogrammed MSCs making them especially attractive in the context of cancer therapy.

Accum® is a cholic acid-nuclear localization sequence (ChAc-NLS) fusion molecule designed to enhance intracellular uptake and release of biomolecules within target cells [40]. The designed properties of Accum® bio-conjugation yielded two distinct benefits of special significance to vaccine development: (1) shorter entrapment and earlier antigen leakage from the endosome, preserving it from excessive degradation, and (2) the enhanced cytosolic delivery of antigens for processing by the proteasomal complex [41, 42], with the latter being a crucial step for antigen cross-presentation by APCs [41, 43, 44]. As a result, a better/wider pool of immunogenic peptides is available for presentation to prime $CD8^+$ T cells and elicit effective anti-tumoral responses [41, 42, 45]. To take advantage of the accumulative properties of Accum®, the parent molecule and selected analogues were evaluated in vaccine design strategies via different approaches. First, Accum® was tested as part of a protein-based vaccine using the human papilloma virus E7 oncoprotein (tested as a prophylactic or therapeutic vaccine) [42]. Second, ex vivo monocyte-derived DCs pulsed with Accum®-bio-conjugated tumor lysate antigens were capable of halting tumor growth in mice when combined with the immune checkpoint inhibitor (ICI) anti-PD-1 [41]. Third, Goncalves et al. evaluated a cellular vaccine composed of MSCs pulsed with antigens in the presence of the A1 molecule (an Accum® variant) [17]. Remarkably, in addition to enhanced protein aggregation, and accumulation within the cytosol, the A1 treatment reprogrammed MSCs into powerful APCs which were referred to as A1-reprogrammed MSCs (ARMs) [17]. Specifically, when a given antigen is admixed with the A1 molecule (an Accum® derivative), protein aggregates are formed prior to their capturing by MSCs via endocytosis. Once in the endosome, the A1 molecule triggers ROS production via NADPH oxidase, which in turn stimulates endosomal membrane lipid peroxidation. At that point, the captured aggregates are released into the cytosol, which is then sensed by the cell, triggering the activation of the UPR in order to eliminate the aggregate via proteasomal degradation [46, 47]. Combined, this resulted in enhanced antigen availability for proteasomal processing [17]. Consequently, the obtained ARM vaccine successfully elicited a potent antitumoral response in mouse models of lymphoma and melanoma, especially using allogenic MSCs in combination with anti-PD-1 [17]. Although the ARM vaccine triggered meaningful anti-tumoral responses resulting in solid tumor regression in almost all animals

with pre-established solid T-cell lymphoma, clinical translation of this approach was challenging, as a minimum antigen dose of 0.5 mg/mL was needed to mount a detectable $CD8^+$ T cell response in vitro [17]. Such a logistical hurdle represents a major barrier, as the generation of a 20–30 million cell dose for a 70 kg patient would require a large tumor sample for the preparation of a tumor lysate solution suitable for in vitro MSC pulsing. To bypass this obstacle, a series of variants were engineered and tested to identify a molecule capable of bypassing the aforementioned antigen dosing limitation while reproducing all, if not most, of the A1 characteristics [17, 48].

In this study, we focus on AccuTOX®, an analogue of Accum®, and its effect on MSCs in the premise of vaccine development. AccuTOX®, and its parent molecule Accum®, have been reported to trigger immunogenic cell death in various murine tumor cell lines [48]. The effect is associated with pronounced endosomal damage, and increased ROS production, along with a potent antigen cross-presentation capacity [48]. When administrated via intratumoral injection, AccuTOX® revealed powerful cytotoxic properties, which synergized with different ICIs at controlling cancer growth [48]. In concordance with the effect of A1 on murine MSCs, the effect of AccuTOX® on MSCs (ARM-X) led to effective antigen cross-presentation and ROS production. The protective immune stimulation using ARM-X was achieved using lower antigen quantities than previously needed with the A1-based ARM strategy, therefore simplifying its logistics for production and clinical translation.

Methods

Mice strains

All in vivo experiments used 6–10-week-old female C57BL/6 mice, or male and female BALB/c mice, purchased from Charles River (Senneville, QC, Canada). Female OT-I mice (6–10 weeks old) were purchased from Jackson Laboratories (Bar Harbor, ME, USA). All mice were housed and maintained in accordance with the guidelines approved by the Animal Care Committee of Université de Montréal in a pathogen-free environment at the animal facility of the Institute for Research in Immunology and Cancer (IRIC). Animal protocols were approved by the Animal Care Committee of Université de Montréal. The work has been reported in line with the ARRIVE guidelines 2.0.

Cell lines and primary cells

The B16F0, Pan02 and CT26 cell lines were purchased from ATCC. The B3Z T-cell line (specific to the SIINFEKL peptide presented in the context of H2-K^b) was a generous gift from Dr. Michel Desjardins (Université de Montréal, Montreal, QC, Canada). B16F0 and CT26 cells were maintained in Dulbecco's modified Eagle's medium (DMEM) supplemented with 10% fetal bovine serum (FBS) and 50 U/mL Penicillin–Streptomycin. Pan02 were cultured in Roswell Park Memorial Institute (RPMI) 1640 supplemented with 10% FBS, 50 U/mL Penicillin–Streptomycin and 1% non-essential amino acids. The B3Z cells were cultured in RPMI 1640 supplemented with 10% FBS, 50 U/mL Penicillin–Streptomycin, 2 mM L-glutamine, 10 mM HEPES, 1 mM Sodium Pyruvate, and 0.5 mM β-Mercaptoethanol. All cells were maintained at 37 °C in a 5% CO_2 incubator. All cell culture media and reagents were purchased from Wisent Bioproducts (St-Bruno, QC, Canada). Human MSCs and their culture medium were purchased from RoosterBio (Frederick, MD, USA) and used according to manufacturer's instructions.

Generation of bone-marrow-derived MSCs

The isolation of murine bone marrow (BM)-derived MSCs were collected as previously detailed [15]. Briefly, femurs of female C57BL/6 or BALB/c mice were flushed with Alpha Modification of Eagle's Medium (AMEM) supplemented with 10% FBS, and 50 U/mL Penicillin–Streptomycin in 10 cm [2] cell culture dish to collect BM cells. Non-adherent cells were removed by changing the media after 24 h then every 3 to 4 days. [14, 15] When a homogenous population was obtained, the cells were collected and assessed for their expression of innate MSC markers (CD44, CD45, CD73, and CD90) by flow cytometry. Validated MSCs were expanded and stored in liquid nitrogen for future use.

Phenotypic analysis by flow cytometry

Phenotypic analysis was conducted as previously reported [15]. Briefly, the cells were collected, counted, and washed with PBS twice. To stain surface markers, the cells were resuspended at the density of 10^5 cells/mL in cold 2% FBS in PBS and incubated with flow cytometry antibodies or their isotypes diluted according to manufacturer's instructions for 30 min at 4 °C in the dark. After washing to remove excess antibodies, stained cells were resuspended in 400 µl of cold 2% FBS in PBS and kept on ice in the dark until they were acquired by BD FACS Diva on CANTOII. The obtained data was analyzed using FlowJoV10.

MSC/ARM-X differentiation into osteoblasts and adipocytes

To assess MSC/ARM-X differentiation capacity, the cells were induced when they reached 60–70% confluency [15, 49]. For osteogenic differentiation, MSCs or ARM-X cells

were cultured for 3–4 weeks in AMEM media supplemented with 10% FBS in addition to β-glycerol phosphate (10 mM), dexamethasone (10^{-8} M), and ascorbic acid 2-phosphate (5 μg/mL). The media was replaced every 2–3 days. Osteogenic differentiation was validated by staining calcium deposits using Alizarin Red S by washing the cells using with phosphate-buffered saline (PBS), followed by incubation for 5 min in 2% Alizarin Red S solution (pH adjusted to 4.1 using ammonium hydroxide), then rinsed with distilled H_2O. A similar approach was used for adipogenic differentiation, except the cells were cultured in AMEM supplemented with 10% FBS, indomethacin (46 μM), 3-isobutyl-methylxanthine (0.5 mM), dexamethasone (1 μM), and insulin (10 μg/mL), changing the media twice over the course of 7 days. Once the differentiation period was completed, oil droplets within differentiated adipocytes were visualized by staining for 10 min using Oil Red O solution prepared by mixing Oil Red O (dissolved at 3.75% in isopropanol) and 2 parts distilled H_2O. At the end of the incubation time, the cells were rinsed with distilled H_2O. The cells were visualized via transmitted light and imaged using EVOS® FL cell imaging microscope (ThermoFisher Scientific).

Identification of the AccuTOX® maximum tolerated dose (MTD)

In order to identify a non-toxic working dose for AccuTOX®, 25×10^4 MSCs/well were plated in a 24-well plate. The following day, various AccuTOX® concentrations (1–50 μM) were added for 24 h. DMSO was used as negative control. The following day, all wells were washed, and then collected to conduct counting using Trypan blue. The highest dose tolerated before evident cell death was selected.

Antigen cross-presentation assay

To assess the cross-presentation ability of the ARM-X cells, we employed two antigen presentation assays using (1) B3Z $CD8^+$ hybridoma T cells ($CD8^+$ hybridoma T cells engineered to express T cell receptors capable of specifically recognizing and responding to the SIINFEKL peptide presented on MHC-I. Successful presentation/cross presentation of SIINFEKL–H-$2K^b$ complexes on the cell surface leads to TCR activation and expression of β-galactosidase by B3Z cells) or (2) primary $CD8^+$ T cells isolated from the spleen of OT-1 transgenic mice.

For the antigen presentation assay using B3Z cells, 25×10^3 MSCs/well were seeded in a 24-well plate. On the following day, MSCs were pulsed for 3 h by adding fresh media containing 1.0 to 0.001 mg/ml of OVA admixed with AccuTOX® (at 25 μM). The positive control group was pulsed with SIINFEKL at 0.1 μg/mL for 3 h. At the end of the pulsing period, the cells were washed with PBS, then 5×10^5 B3Z cells were added per well for 17–19 h. Once the incubation period was completed, the media was removed, and the cells were washed once with PBS and lysed using lysis buffer (tris base, CDTA, glycerol and triton X-100) on a shaker for 20 min at room temperature. Cell lysate was then incubated with a CPRG solution (containing CPRG, disodium phosphate, monosodium phosphate, potassium chloride, magnesium sulfate) and protected from light for 24 h at 37 °C. The optical density signal was detected at wavelength 570 nm using a SynergyH1 microplate reader (Biotek, Winooski, VT, United States). The optical density at 570 nm corresponds to the cleavage of CRPG, which is directly proportional to the degree of β-galactosidase activity, and therefore, B3Z activation. For experiments evaluating the effects of ROS neutralization on AccuTOX®-induced cross-presentation, the same antigen cross-presentation assay described above using the B3Z cell line was performed but with selected inhibitors added at the same time as the AccuTOX® molecule. Following 6 h of incubation, the cells were washed and 5×10^5 B3Z cells were added per well. In addition to using N-Acetyl Cysteine (NAC—5 mM) as a general ROS inhibitor, MitoTEMPO (10 μM) was used as a specific mitochondrial ROS inhibitor, whereas α-tocopherol (2 mM) was tested as a blocker for lipid peroxidation. The NOX inhibitors Diphenyleneiodonium chloride (DPI) and 2-Acetylphenothiazine (ML171) were used at (20 μM) respectively. A similar approach was used when ARM-X were treated with the unfolded protein response (UPR) inhibitors, trazodone (1, 5, 10, and 20 μM), salubrinal (5, 10, 25, and 50 μM), KIRA8 (2.5, 5, 10, 20, and 40 nM) and AEBSF (75, 150, 300, and 600 μM).

For the assay using OT-I-derived $CD8^+$ T cells, the same overall parameters were used except that at the end of the pulsing period, the cells were co-cultured with 10^6/ml $CD8^+$ T-cells purified from the spleen of OT-I male mice (6–10 weeks old) using the $CD8\alpha^+$ positive isolation kit according to the manufacturer's protocol. Three days later, supernatants were collected, centrifuged for 5 min at 1500 rpm, 4 °C to remove cell debris and used to quantify IFNγ levels by ELISA (R&D).

Monitoring antigen uptake and processing

To evaluate antigen uptake, 5×10^4 MSCs/well were seeded in a 12-well plate. On the following day, the cells were treated with 1 μg/ml of Alexa Fluor® 647-conjugated OVA (a fluorescent OVA conjugate) admixed with AccuTOX® for 3 h at 37°C. The cells were then collected, washed with PBS before the assessment of their

fluorescence by flow cytometry. To evaluate antigen processing, MSCs were incubated with 10 µg/mL DQ™ Ovalbumin (a self-quenched conjugate of OVA that emits fluorescence upon processing) admixed with AccuTOX® at 37°C. One hour later, cells were washed, and regular media was added for 3 h. At the end of the indicated incubation, cells were collected to assess their fluorescence using BD FACS Diva on CANTO II.

Assessing endosomal escape

To evaluate endosomal escape, we used a previously established in vitro assay assessing Cytochrome (Cyt)-C-induced apoptosis [50]. Briefly, 10^5 MSCs/well were seeded in a 6-well plate prior to supplementing them with 10 mg/mL of exogenous Cyt-C for 6 h at 37°C in the presence or absence of AccuTOX® (25 µM). At the end of incubation period, the cells were washed and collected using Accutase® prior to Annexin-V staining and analysis using BD FACS Diva on CANTO II.

Evaluating ROS production

Analysis of mitochondrial ROS production in ARM-X treated cells was evaluated by MitoSOX staining according to manufacturer instructions. Briefly, 25×10^3 cells/well were seeded in a 12-well plate. The following day cells were treated with 25 µM AccuTOX® in the presence or absence of NAC (5 mM), DPI (20 µM), ML171 (20 µM), MitoTEMPO (10 µM) or α-tocopherol (800 µM). After incubation, the cells were washed with PBS, collected using trypsin, washed with ice-cold 2% FBS in PBS solution, then stained with MitoSOX (5 µM diluted in PBS) for 30 min at 37 °C. After staining, cells were washed once with ice-cold 2% FBS in PBS solution. The stained cells were resuspended in 2% FBS in PBS solution and kept on ice in the dark to be analyzed by BD FACS Diva on CANTO II within 1 h.

Cytokine and chemokine analysis

To assess the profile of cytokine and chemokine production, ~ 1.0×10^6 MSCs were grown in serum-free AMEM for 24 h. MSCs were then treated with 25 µM of AccuTOX® in serum-free AMEM for 24 h. The post-treatment supernatant was collected and kept at 4 °C, and fresh serum-free AMEM was replenished without AccuTOX®. After 24 h of the initial AccuTOX® treatment, the supernatant was collected and added to the previous collection. All collected supernatant was combined and concentrated 80× using the Amicon Ultra-4 centrifugal filters (3000 NMWL) for 1 h at 4 °C at 4500×*g*. Collected concentrates were then aliquoted and frozen at − 80 °C until shipped to EveTechnologies (Calgary, AB, Canada) for cytokine/chemokine assessment by Luminex.

Dynamic light scattering (DLS) analysis of protein aggregates

DLS measurements were carried out on a Malvern Zetasizer Nano ZSP. All samples were measured in disposable Malvern PMMA cuvettes, 1 cm path length. Measurements were taken at 25 °C in triplicate. All samples were vortexed for 30 s to ensure homogeneity prior to analysis. Hydrodynamic size and polydispersity were calculated using the cumulants analysis method in the Zetasizer software.

Analysis of cell persistence post-injection

The live in vivo imaging study was designed to evaluate the persistence of ARM-X cells in vivo. For this experiment, MSCs transduced to stably express the firefly luciferase gene. Once the ARM-X cells were generated using AccuTOX®, female and male Balb/c mice (n = 6/group/sex) were subcutaneously (SC)-injected with 0.5, 1.0 or 2×10^6 ARM-X cells. The bioluminescence signal was recorded at days 1, 3 and 5 post injection. For each imaging session performed at the IRIC (Université de Montréal, Montreal, QC), mice received an IP injection of 0.2 ml of 15 mg/ml XenoLight D-Luciferin—K + Salt (equivalent to 30 mg/kg). Mice were kept under 1.5–2.5% inhaled isoflurane anesthesia and the bioluminescence signal was acquired after 10 min using the Prism in vivo imaging system (Médilumine, QC, CANADA). The acquired data were then plotted as luciferase signal decay.

Generation of tumor lysates

To prepare cell lysates, cultured cancer cells were collected using 0.05% trypsin then washed 3 times with PBS in centrifugation cycles of 1000 rpm for 10 min to remove traces of FBS. Washed cells were kept as a pellet at − 80 °C until lysis. To induce cell lysis, the cell pellet was subjected to 5 cycles of freezing in liquid nitrogen followed by thawing (at 37 °C) cycles, with complete homogenization with vortex/shaking conducted before every freezing/thawing step. The final solution was centrifuged for 10 min at 4500×*g* at 4 °C and the protein lysate supernatant was collected, quantified, aliquoted and stored at − 80 °C until further use. Protein quantification was performed using Bio-Rad Protein Assay (Bio-Rad) according to manufacturer instructions.

Cell-based vaccination studies

To generate the allogeneic ARM-X vaccine, culture-adapted MSCs (derived from C57BL/6 or Balb/c) were pulsed with fresh media containing the antigen (0.5 or 0.05 mg/mL tumor lysate) with or without AccuTOX® (25 µM) for 24 h. Once pulsing was completed, the cells were washed with PBS, detached using Accutase®,

then counted to obtain 5×10^5 cells/100 µL. The used tumor cells were similarly counted and washed three times using PBS. To evaluate the therapeutic properties of ARM-X, female C57BL/6 and Balb/c mice (n = 10/group) were SC-injected with 5×10^5 B16F0 or CT26 cells, respectively at day 0 on the hind. At days 3 and 10, the mice were intratumorally SC-injected (at distal site from the tumor) with 5×10^5 ARM-X cells. Control animals received 5×10^5 tumor cells alone. For the Pan02 model, 2×10^6 cells (diluted in 100 µL PBS) were admixed to 100 µL Matrigel™ on ice before SC transplantation in C57BL/6 mice. To assess the effectiveness of the therapeutic vaccine as a combination therapy with immune-checkpoint inhibitor anti-PD-1, starting day 10, the mice start receiving intraperitoneal (IP) injections of the antibody or its isotype at 200 µg per dose every 2 days for a total of 6 doses over two weeks. For in vivo studies related to phagocyte depletion, animals were IP-injected with a clodronate solution (0.5 mg/mL) 24 h prior to ARM-X administration. Studies related to the depletion of CD4, CD8, CD19 and NK1.1, specific antibodies were administered via the IP route at 200 µg per dose every 2 days, for a total of 3 doses, one week before tumor implantation. All animals were followed for tumor growth using a digital caliper for 6 weeks or until reaching endpoints (ulceration or a tumor volume ≥ 1000 mm^3). Mice were euthanized through carbon dioxide (CO_2) inhalation.

RNA-Seq alignment and differential expression analysis

To conduct the transcriptomic study, murine and human MSCs were treated with 10 µM AccuTOX® for 24 h. At the end of treatment period, the cells were detached, washed, and collected to extract their RNA using the RNeasy Mini Kit (QIAGEN). Quantification of total RNA was made by QuBit (ABI), and 500 ng of total RNA was used for library preparation. The quality of total RNA was assessed with the BioAnalyzer Nano (Agilent), and all samples had a RIN above 8. Library preparation was done with the KAPA mRNAseq stranded kit (KAPA, Cat no. KK8420). Ligation was made with 9 nM final concentration of Illumina index, and 10 PCR cycles were required to amplify cDNA libraries. Libraries were quantified by QuBit and BioAnalyzer. All libraries were diluted to 10 nM and normalized by qPCR using the KAPA library quantification kit (KAPA; Cat no. KK4973). Libraries were pooled to equimolar concentration. Sequencing was performed with the Illumina Hiseq2000 using the Hiseq Reagent Kit v3 (200 cycles, paired-end) using 1.7 nM of the pooled library. RNA sequencing data in FASTQ format were aligned to the reference genome using the STAR aligner (v2.7), employing recommended parameters for accurate and efficient alignment. Gene-level read counts were quantified from the aligned BAM files and processed with DESeq2, following best practices for normalization, dispersion estimation, and statistical testing. Differentially expressed genes (DEGs) were identified based on a significance threshold of log2 fold change ≥ 0.5 and an adjusted p value of ≤ 0.05, unless stated otherwise.

Downstream analysis and visualization

Gene set enrichment analysis (GSEA) was performed on the list of DEGs to identify enriched pathways and biological processes. Peptide binding affinities from immunopeptidomic experiments were predicted using NetMHCpan 4.0. Data visualizations, including heatmaps, pathway enrichment plots, and other graphical summaries, were created using R packages such as pheatmap, clusterProfiler, and ggplot2, complemented by custom R scripts for further analysis.

Immunopeptidome analysis

To investigate the impact of AccuTOX® on the peptide repertoire of human MSCs was conducted as previously described [15]. Briefly, MSCs treated as previously described were detached using Accutase®, then washed 3 times with PBS prior to snap-freeze in liquid nitrogen (about 50×10^6 cells were pelleted per condition). Following pellet lysing using a 1% Triton X-100-based buffer, obtained lysates were incubated with 200 µg M1/42 linked to CNBr-activated sepharose overnight to immunoprecipitate mouse MHC class I, then washed with lysis buffer followed by Tris–HCl with decreasing NaCl concentrations. The final elution was carried out in LoBind Eppendorf tubes using 0.1 M acetic acid and 0.1% TFA. Peptides were concentrated and desalted using solid-phase extraction (SPE) with an Empore C18 plate. Peptides were loaded directly and eluted using 80/20 acetonitrile/water (0.1% TFA). Eluted peptides were lyophilized and reconstituted in 0.1% TFA. Peptides (50% per sample) were analyzed by nano LC/MS/MS using a Waters NanoAcquity system interfaced to a ThermoFisher Fusion Lumos mass spectrometer. Peptides were loaded on a trapping column and eluted over a 75 µm analytical column at 350 nL/min; both columns were packed with Luna C18 resin (Phenomenex). A 2-h gradient was employed. The mass spectrometer was operated using a custom data-dependent method, with MS performed in the Orbitrap at 60,000 FWHM resolution and sequential MS/MS performed using high resolution CID and EThcD in the Orbitrap at 15,000 FWHM resolution. All MS data were acquired from m/z 300–800 (Class I) and m/z 300–1500 (Class II). A 3 s cycle time was employed for all steps. Peptide analysis was conducted using the free online analysis tools GibbsCluster and NetMHCpan to stratify the peptides identified in the immunopeptidome sequencing. Binding affinity predictions

are classified by the percentage rank with strong binding (SB) = < 0.5%; moderate biding (MB) = 0.5%–2.0%; and weak binding (NB) = > 2.0%.

Statistical analysis

P values were calculated using one-way analysis of variance (ANOVA) or Log-rank test for animal survival experiments. Results are represented as average mean with standard deviation (S.D.) error bars, and statistical significance is represented with asterisks: $^{*}p < 0.05$, $^{**}p < 0.01$, $^{***}p < 0.001$.

Results

AccuTOX® retains most of the A1 properties while lowering the needed concentration for antigen pulsing

The use of the A1 Accum® derivative for the preparation of the first-generation ARM vaccine was instructive in terms of the requirements needed to successfully convert innate MSCs into potent APCs [17]. These requirements include the need of a compound eliciting: (1) no cellular toxicity, (2) endosomal breaks for antigen release into the cytosol, (3) activation of the antigen cross-presentation machinery (e.g. enhanced antigen uptake and processing), and (4) the retention of the innate MSC phenotype (Fig. 1a). When screening Accum® derivatives using these established parameters, we identified AccuTOX® (a hybrid CDCA bile acid fused to the SV40 peptide) as the ideal lead compound (Fig. 1b). For instance, an MTD analysis conducted using various AccuTOX® concentrations identified 25 µM as the ideal working dose due to its limited interference with MSC proliferation (Fig. 1c) and absent cell death (Fig. 1d). Furthermore, AccuTOX®-reprogrammed MSCs (ARM-X): (1) retain the same phenotype as untreated cells by expressing CD44, CD73, CD90, H2-K^b and PD-L1 markers, while remaining negative for CD45 expression (Fig. S1A), (2) have a similar cytokine secretion profile compared to control innate MSCs (Fig. S1B), and (3) efficiently differentiate into adipocytes (Fig. S1C) and osteoblasts (Fig. S1D) upon appropriate stimulation. Furthermore, the use of AccuTOX® at 25 µM triggered optimal antigen cross-presentation as depicted by the cells' ability to activate the SIINFEKL-specific B3Z T-cell line in response to ovalbumin (OVA) pulsing (Fig. 1e). In contrast, the highest AccuTOX® dose of 50 µM killed all cells (Fig. 1e). Utilizing the optimal dose of 25 µM, we next tested the lowest OVA concentration needed to trigger a detectable in vitro T-cell response and found similar B3Z activation in response to OVA concentrations ranging from 1.00 to 0.05 mg/mL (Fig. 1f), an observation further confirmed using primary OT-I-derived $CD8^+$ T cells (Fig. 1g). Since AccuTOX® treatment of MSCs is usually conducted over a period of 24 h, we next assessed whether a shorter treatment time could convert MSCs into ARM-X cells. Compared to the results obtained using a 24-h treatment time (Fig. 1e–g), MSCs pulsed with OVA admixed with AccuTOX® for 6 h show no B3Z response (Fig. 1h). In addition, the generated ARM-X cells should be used in less than 24 h post-AccuTOX® treatment, as no detectable B3Z response could be observed at longer time points (Fig. S2A). Since the latter point is important logistically, we next conducted an experiment testing the cross-presenting ability of ARM-X cells following a cycle of freeze and thaw to mimic clinical settings (Fig. S2B). When ARM-X cells are thawed and then plated to allow for cellular adhesion prior to B3Z co-culture, no response could be detected (Fig. S2C), which is consistent with the timeline study presented in Fig. S2A. On the other hand, co-culturing thawed ARM-X cells directly with B3Z triggers a detectable but weaker response (~ 40–50% of the initial response) compared to freshly generated ARM-X cells (Fig. S2C). Finally, we compared the antigen uptake and processing abilities of ARM-X cells to innate MSCs using Alexa Fluor® 647-conjugated OVA and DQ™-Ovalbumin respectively. [15, 17] Interestingly, enhanced antigen uptake (Fig. 1i) and processing (Fig. 1j) were observed in ARM-X cells across all tested doses, indicating a positive stimulating impact for AccuTOX® on the initial steps governing antigen cross-presentation.

One of the main characteristics for Accum® and its derivatives is ROS induction in target cells [17, 41, 48, 51]. Given that AccuTOX® is no different in that regard, as it triggers a strong ROS production in treated MSCs (Fig. 1k), we next analyzed the neutralizing effect of various antioxidants on ROS production in ARM-X to identify their potential source. ROS levels were strongly inhibited using NAC, as well as DPI and ML171 (inhibitors of NADPH oxidases—Fig. 1k). The observations obtained with both NADPH oxidase inhibitors are consistent with an absent effect for mitochondria-induced ROS production, as ARM-X treatment with MitoTEMPO (mitochondrial ROS inhibitor) showed no impact on ROS levels (Fig. 1k). In contrast, moderate inhibition of ROS production was observed using the lipid peroxidation inhibitor α-tocopherol (Fig. 1k). To further highlight the link between AccuTOX®-mediated endosomal membrane breaks via ROS/lipid peroxidation and T-cell activation, a cross-presentation experiment was conducted using ARM-X cells treated with ML171 or DPI. A significant decrease in B3Z T-cell activation was observed (Fig. 1l), clearly indicating that endosomal ROS production triggered by AccuTOX® is central to the release of captured antigens into the cytosol. We also confirmed this notion using an in vitro assay assessing the impact of intracellular endosomal release of recombinant Cyt-C [50] (Fig. 1m) and found that it was indeed the case

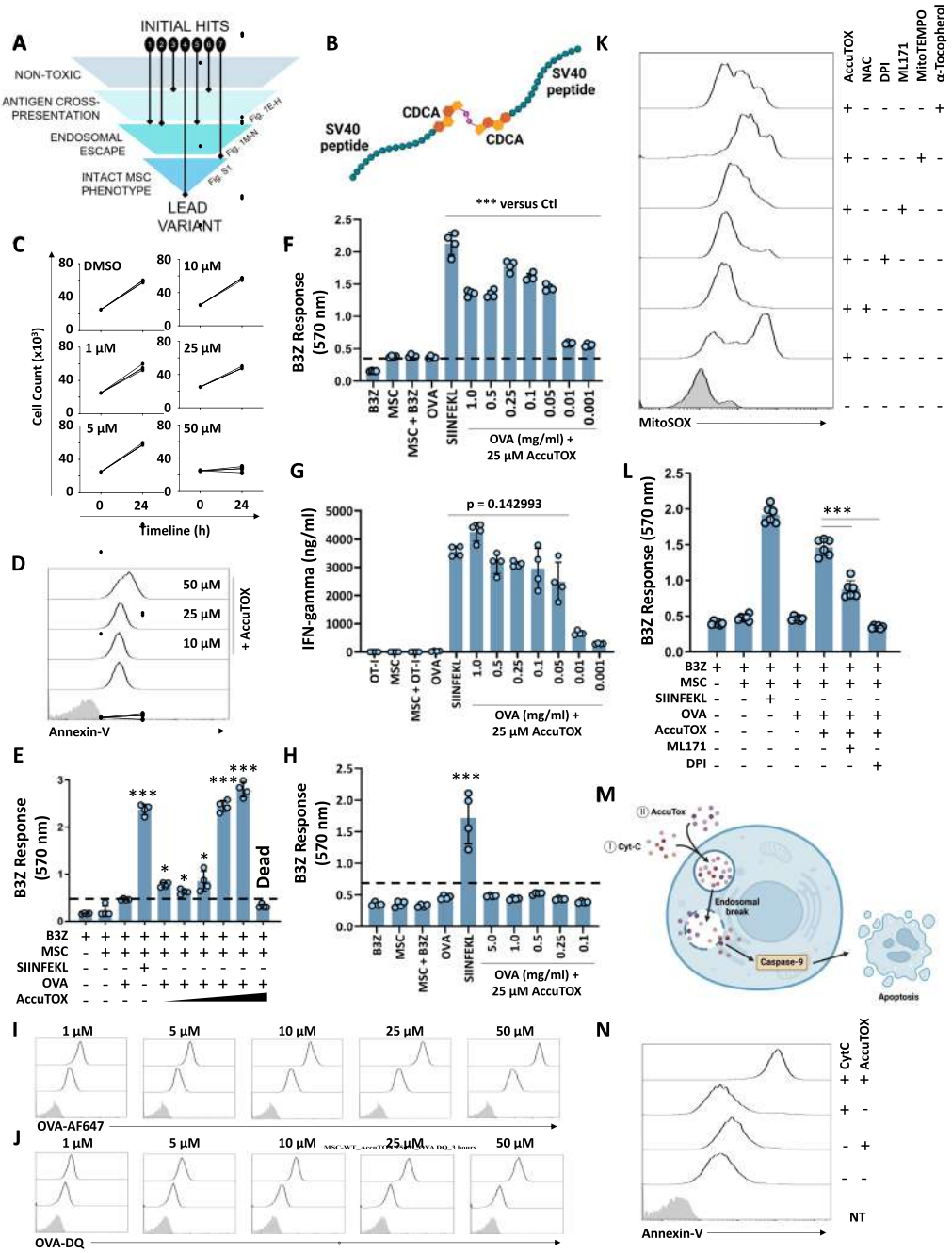

Fig. 1 Characterising the cross-presenting ability of murine ARM-X cells. **a** schematic diagram depicting the parameters used for selecting the Accum® derivative needed for MSC reprogramming. **b** Graphical depiction of the predicted structure of AccuTOX®. **c** An MTD experiment conducted on murine MSCs using various AccuTOX® concentrations. **d** A representative flow cytometry analysis of Annexin-V staining conducted on MSCs treated with various AccuTOX® concentrations. **e** In vitro cross-presentation experiments conducted on MSCs treated for 24 h with various AccuTOX® concentrations. **f** An in vitro cross-presentation experiments conducted on MSCs treated with a fixed AccuTOX® dose (25 µM) admixed with descending OVA concentrations using the B3Z T-cell line. **g** Similar to panel (**f**) but using OT-I-derived $CD8^+$ T cells as responding T cells. **h** Same as panel (**f**) except that MSCs were treated with 25 µM of AccuTOX.® for 6 h. **i** A representative flow cytometry analysis depicting fluorescent OVA Alexa Fluor™ 647 (OVA AF-647) uptake by MSCs (lower histogram panels) versus ARM-X (upper histogram panels). **j** Same as (I) but for assessing antigen processing using DQ™ ovalbumin (OVA-DQ). **K)** A representative flow cytometry analysis for ROS production in the absence or presence of various antioxidants. **l** An in vitro cross-presentation experiment conducted in the presence of antioxidants. **m** A graphical depiction of the assay used to assess endosomal escape. **n** A representative flow cytometry analysis depicting apoptosis induced by endosomal escape. For panel C, n = 3/group. For panels E, F, G, H, and L n = 4–6/group with $*P < 0.05$; and $***P < 0.001$

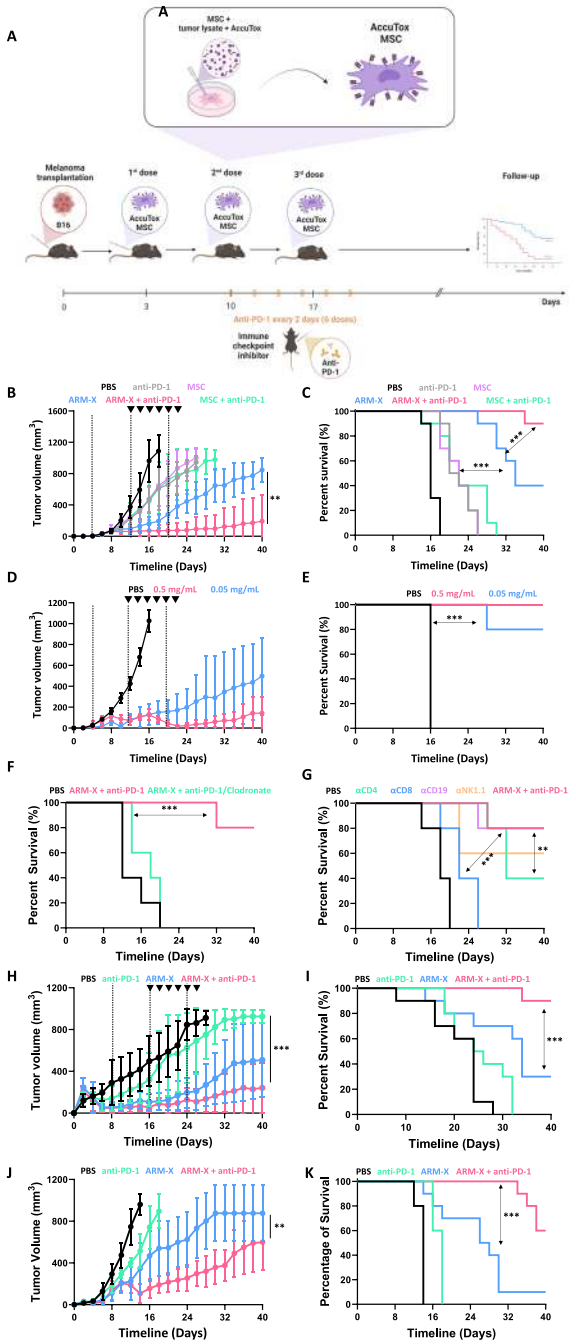

◀ **Fig. 2** ARM-X administration impairs the growth of multiple solid tumors. **a** Schematic depiction of the therapeutic vaccination approach used for all cancer models. **b** Therapeutic vaccination using the B16F0 tumor lysate at 0.5 mg/ml. Control mice are shown in black; anti-PD-1 in purple; MSCs pulsed with tumor lysate in gray; MSCs pulsed with tumor lysate and anti-PD-1 in green; ARM-X in blue; and ARM-X and anti-PD-1 in red. The black dotted lines represent therapeutic vaccination using cells whereas the black triangles depict anti-PD-1 injections. **c** The survival curve for the experiment displayed in panel B. **d** Therapeutic vaccination comparing ARM-X pulsed with 0.5 mg/mL (red) versus 0.05 mg/mL (blue) of B16F0 tumor lysate. Control mice are shown in black. **e** The survival curve for the experiment displayed in panel D. **f** Survival curve of a therapeutic vaccination trial using ARM-X and anti-PD-1 pulsed with 0.05 mg/ml of B16F0 tumor lysate and in animals pre-treated with clodronate (green) versus liposome control (red). Control mice are shown in black. **g** Survival curve of a therapeutic vaccination trial using ARM-X pulsed with 0.05 mg/ml of B16F0 tumor lysate in animals pre-treated with depleting antibodies targeting CD4 (green), CD8 (blue), CD19 (purple), and NK1.1 (orange). Non-depleted mice receiving the ARM-X vaccine and anti-PD-1 are in red whereas control mice are shown in black. **h** Therapeutic vaccination using ARM-X pulsed with 0.05 mg/ml of Pan02 tumor lysate. Animals treated with anti-PD-1 are shown in green, ARM-X in blue and ARM-X with anti-PD-1 in red. Control mice are shown in black. **i** Survival curve of the experiment shown in panel (**h**). **j** Therapeutic vaccination using ARM-X pulsed with 0.05 mg/ml of CT26 tumor lysate. Animals treated with anti-PD-1 are shown in green, ARM-X in blue and ARM-X with anti-PD-1 in red. Control mice are shown in black. **k** Survival curve of the experiment shown in panel (**j**). For this experiment, n = 10/group with $^{**}P < 0.01$, and $^{***}P < 0.001$

(Fig. 1n). Altogether, this set of experiments demonstrates that AccuTOX® reprograms MSCs into potent APCs while retaining most of the functions displayed by the original A1 Accum® derivative.

The ARM-X vaccine impairs the growth of pre-established solid tumors

In light of the antigen cross-presenting activities mediated by AccuTOX® treatment of MSCs, we next studied the therapeutic potency of these cells in various solid tumor models. To begin, we treated C57BL/6 mice harboring pre-established B16F0 tumors with three allogeneic ARM-X doses as a monotherapy or in combination with anti-PD-1 antibodies (Fig. 2a). Indeed, the use of the standard high tumor lysate pulsing dose (0.5 mg/mL) triggered potent therapeutic effects as depicted by a blockade in B16F0 growth (Fig. 2b; Fig. S3A) resulting in a 90% survival rate by day 40 post-vaccination (Fig. 2c). We next compared this formulation to the lowest lysate dose of 0.05 mg/mL and found the latter to trigger a meaningful therapeutic response (Fig. 2d) resulting in an 80% survival rate compared to 100% using the 0.5 mg/mL OVA dose (Fig. 2e). Interestingly however, therapeutic vaccination using the first-generation ARM vaccine pulsed with the low antigen dose resulted in a weaker therapeutic effect compared to ARM-X (Fig. 3SB) with a 0% survival rate compared to 100%, respectively (Fig. S3C). This led us to question whether the ARM-X cells pulsed with different OVA doses affect the T-cell activation thresholds, leading to this drastic difference in survival. To test that hypothesis, two groups of immunocompetent C57BL/6 mice were administered three doses of the ARM-X cells pulsed with high (0.5 mg/mL) or low (0.05 mg/mL) tumor lysate to generate antigen-specific

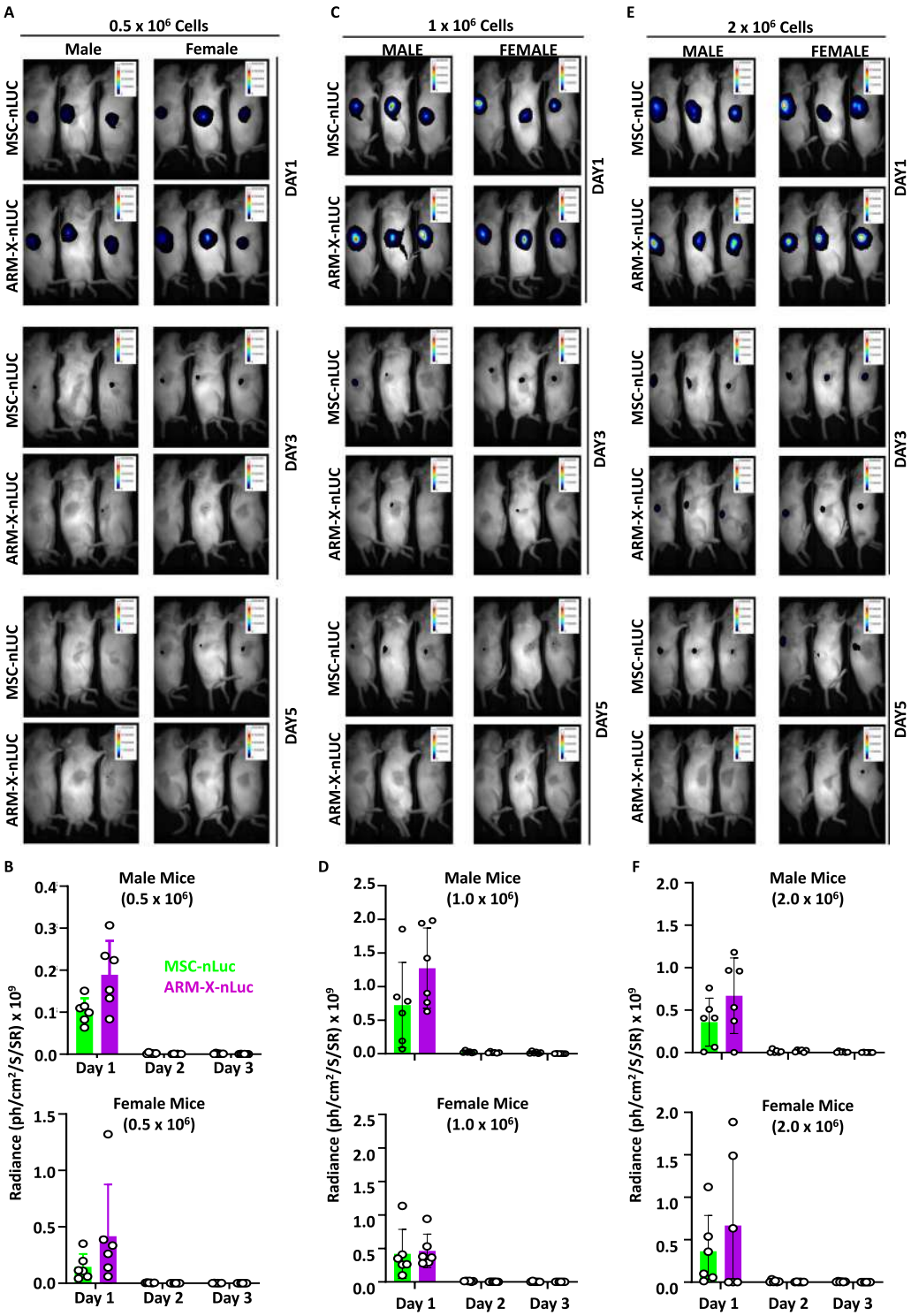

Fig. 3 ARM-X cells administered to immunocompetent mice are cleared shortly after injection. **a** Representative live in vivo imaging of male and female Balb/c mice implanted with luciferase(nLUC)-expressing control MSC-nLUC versus ARM-X-nLUC injected at a dose of 0.5×10^6 cells. **b** Assessment of the signal decay for the experiment shown in panel (**a**). **c** Same as panel (**a**) but using a dose of 1.0×10^6 cells. **d** Assessment of the signal decay for the experiment shown in panel (**c**). **e** Same as panel (**c**) but using a dose of a dose of 2.0×10^6 cells. **f** Assessment of the signal decay for the experiment shown in panel (**e**). For this experiment, n = 6/group/sex

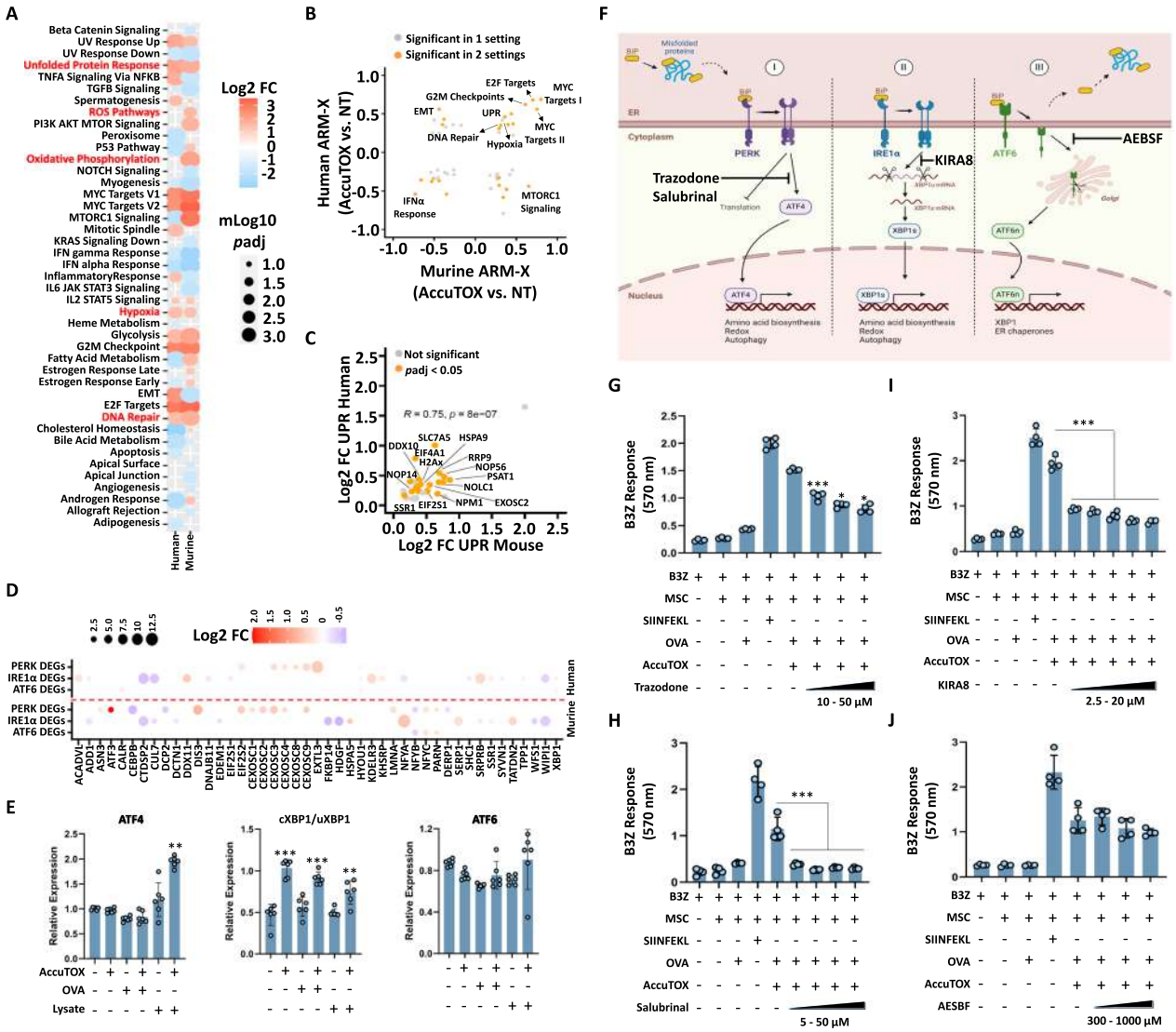

Fig. 4 The cross-presentation of ARM-X depends on the UPR. **a** The gene set enrichment analysis for both human and murine ARM-X (AccuTOX.® versus non-treated MSCs). Hallmark gene sets that are significant in at least one dataset are shown on the y-axis. Positive enrichment scores are depicted in red, while negative enrichment scores are represented in blue. The size of the dots corresponds to the significance of the adjusted p-values, displayed on a -log10 scale. **b** Scatter plot illustrating the correlation between hallmark gene sets from human and murine ARM-X datasets. Gene sets significant in both datasets (adjusted *p* value < 0.05) are highlighted in orange. Labeled points represent hallmark gene sets of interest, which are either significantly upregulated or downregulated in both datasets or show opposing regulation (upregulated in one and downregulated in the other). **c** Scatter plot displaying the correlation of genes significantly regulated within the UPR hallmark between human and murine ARM-X datasets. The log2 fold changes for human and murine differentially expressed genes are plotted on the y-axis and x-axis, respectively. Genes of interest, which meet the criteria of logFC ≥ 0.5 and adjusted *p* value < 0.05 in both datasets, are labeled. **d** This dot plot highlights three cellular reactome sub-processes related to the UPR and their corresponding significant genes, which are either upregulated or downregulated in murine or human ARM-X datasets. The colors indicate the directionality of the log2 fold change, while the size of the dots represents the significance of the adjusted *p* values from DESeq2 analysis, presented on a -log10 scale. **e** Transcript quantification of the main genes involved in the PERK, IRE1α and ATF6 branches of the UPR in ARM-X cells in response to different antigen treatments. **f** A schematic depiction of the three UPR pathways and the mode of action of the selected drugs. **g** A cross-presentation assay using ARM-X treated with Trazodone. **h** Same as (**g**) but using Salubrinal. **i** Same as (**h**) but using KIRA8. **j** Same as (**i**) but using AESBF. For panels E to J, n = 4 – 6 per group with **P* < 0.05, ***P* < 0.01, and ****P* < 0.001

CD8$^+$ T cells (Fig. 4SA). Isolation and co-culturing of CD8$^+$ T cells from the high antigen dose group strongly responded to ARM-X cells pulsed with 0.5 mg/mL antigen and responded to a weaker extent (50% less) when co-cultured with 0.05 mg/mL pulsed ARM-X cells (Fig. S4B). On the other hand, CD8$^+$ T-cells derived from animals immunized with ARM-X pulsed with the low antigen dose (0.05 mg/mL) responded with a low but similar

magnitude to ARM-X pulsed with both antigen doses (Fig. S4C). These results imply that pulsing ARM-X cells with a given antigen dose has a direct impact on T-cell activation thresholds in vivo.

Prior to testing the potency of the ARM-X vaccine in other tumor models, we next asked whether the vaccine relies on endogenous phagocyte-mediated efferocytosis to mediate its therapeutic effect. To validate this hypothesis, the same vaccination scheme used with the low tumor lysate dose was repeated, but in animals pretreated with clodronate (a phagocyte-depleting drug) versus control liposomes [15, 52] As anticipated, allogeneic ARM-X cells lost their capacity to mount an anti-tumoral effect against established B16F0 tumors when animals are depleted from phagocytes (Fig. 2f). Moreover, antibody-mediated depletion of other immune subsets revealed an important role for $CD8^+$ T cells in the generation of anti-tumoral responses with substantial effects seen for $CD4^+$ T cells (Fig. 2g). Depletion of NK or B cells, on the other hand, had limited impact on animal survival, highlighting a major role for T-cell-mediated adaptive immunity (Fig. 2g). To further demonstrate the versatility of the ARM-X vaccine, we conducted additional vaccination trials targeting two different solid tumors. When tested against the Pan02 pancreatic cancer, animals treated with the ARM-X/anti-PD-1 combination (red line) led to strong therapeutic effects, followed by the ARM-X monotherapy (blue line) with no major impact observed when the anti-PD-1 antibody was delivered alone (Fig. 2h). This correlated with the survival curve, as the combinatorial therapy resulted in 90% survival, followed by 30% with the ARM-X monotherapy while all remaining groups succumbed by days 28–32 (Fig. 2i). Similar outcomes were observed using the CT26 colon cancer model where the combinatorial treatment (red line) greatly impaired tumor growth compared to the ARM-X monotherapy group (blue line—Fig. 2j) with a 60% versus 10% survival, respectively (Fig. 2k). To discern any possible sex-biased effect, therapeutic vaccination against colon cancer was compared in male versus female immunocompetent mice. Interestingly, the combination therapy controlled CT26 tumor growth in both sexes, with slightly enhanced potency in female mice (Fig. 5SA-B). Altogether, these results highlight three important facts: (1 generation of the ARM-X vaccine using a low antigen dose can trigger potent anti-tumoral activity, (2) the therapeutic effect of allogeneic ARM-X cells requires efferocytosis by endogenous phagocytes as well as T-cell-mediated adaptive immunity (both $CD8^+$ and $CD4^+$ T cells), and (3) the ARM-X vaccine is easily adaptable to different solid tumors given access to tumor lysate is granted.

ARM-X cells are rapidly cleared after their administration to immunocompetent mice and show no sign of toxicity

Accumulating research data focuses on efferocytosis of MSCs upon their administration to immunocompetent mice as a central hallmark of their therapeutic mode of action [42, 53–55]. Therefore, it is logical to ask whether administered allogeneic ARM-X cells exhibit a different clearance or migration pattern upon their in vivo administration compared to innate MSCs. To test this hypothesis, luciferase-expressing allogeneic MSCs or ARM-X cells were subcutaneously (SC) injected at different doses (0.5, 1.0 or 2.0×10^6 cells) in both male and female immunocompetent Balb/c mice and the signal was tracked and analyzed using live in vivo imaging over a 5-day period. Although, for both ARM-X and MSCs, the great majority of cells are cleared from both male and female mice on day 1, independent of cell doses (Fig. 3), limited detectable signals could be seen for the two highest doses of 1.0 and 2.0×10^6 cells on days 3 and 5, confirming incomplete clearance at these timepoints (Fig. 3a, c and e). As for differences in the clearance of control MSCs versus ARM-X, both male and female mice receiving 1.0 or 2.0×10^6 MSCs show qualitative delays in clearing the control cells, compared to ARM-X (Fig. 3a, c and e). Thus, we can conclude based on this experiment that ARM-X cells do not exhibit a differential migration pattern, nor a delay in their in vivo clearance.

Besides assessing their clearance rate, we next investigated the safety profile of these cells, especially since they are pulsed with tumor lysate that may contain both self and non-self antigens derived from the CT26 colon cancer cell line as a working example. No differences in animal weight were observed for both male (Fig. S6A) and female (Fig. S6B) populations, as both animal groups gained weight over time. In addition, several toxicological parameters were assessed, including unusual signs at the site of injection or any other pathological sign related to daily animal activities. Since the vaccine was delivered three times, animals were assessed 24 h following each ARM-X administration and were given a score of 0 (no sign), 1 (mild sign), 2 (moderate sign), 3 (strong sign) or 4 (excessive/moribund sign) for each parameter. Besides some minor inflammatory signs at the site of injections for some male (Fig. S6C) and female mice (Fig. S6D) following the first 2 injections, no pathological signs could be observed with respect to the overall activity of the animal, changes to fur or body posture, as well as weight.

AccuTOX® activates the unfolded protein response (UPR) in ARM-X cells

To gain deeper insights into the processes involved in reprogramming MSCs into potent APCs (ARM-X), we conducted a transcriptomic study comparing murine

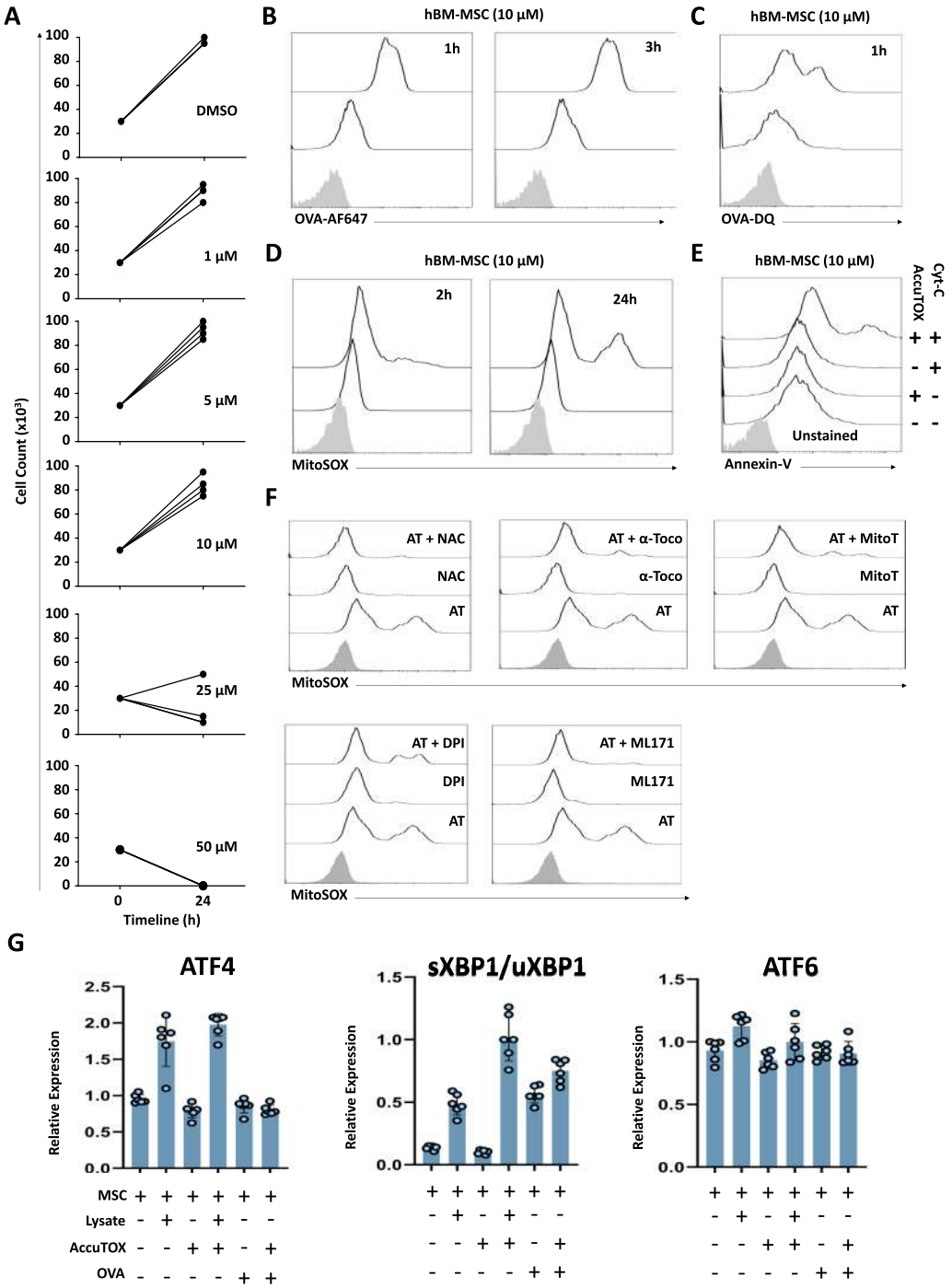

Fig. 5 AccuTOX® effect on human ARM-X cells intersects with the murine ARM-X mode of action. **a** An MTD experiment for AccuTOX® conducted on human MSCs. **b** Representative flow cytometry experiments assessing antigen uptake by human ARM-X upon 1- or 3-h treatment with OVA- Alexa Fluor™ 647 (OVA-AF647). **c** A representative flow cytometry experiment assessing antigen processing by human ARM-X upon OVA-DQ treatment. **d** Flow cytometry analysis of ROS production by human ARM-X upon 2 h or 24 h treatment with AccuTOX®. **e** Flow cytometry analysis of Annexin-V staining in human ARM-X to assess endosomal escape. **f** Flow cytometry analysis of ROS neutralization by various anti-oxidant molecules in human ARM-X cells. **g** Transcript quantification of UPR-associated genes in human ARM-X cells upon treatment with OVA/lysate in the presence or absence of AccuTOX®

and human ARM-X cells to identify commonly modulated pathways. Gene set enrichment analysis using the Hallmark gene set collection (Fig. 4a) revealed over 40 significant hallmark pathways in either human or murine ARM-X cells compared to controls, with the UPR, hypoxia, and DNA repair pathways consistently upregulated in both species (Fig. 4a). Further analysis demonstrated that these three pathways exhibited significant correlations between the two species (Fig. 4b). Given the critical role of the UPR as a cellular defense mechanism against protein aggregation, we next identified several key genes (e.g., *Hspa9*, *Slc7A5*, *Ddx10*, *Eif4a1*, *H2ax*, *Nop14*, *Eif2s1*, *Npm1*, *Nolc1*, *Psat1*, *Exosc2*, and *Rrp9*) that were significantly correlated and differentially expressed in both species in response to ARM-X. These genes are known to play pivotal roles in protein unfolding, amino acid transport, chromatin remodeling, RNA processing or translation regulation, ribosome biogenesis, and DNA repair (Fig. 4c) [46, 47, 56–58]. To further refine our analysis of the UPR pathways, we focused on three cellular reactome sub-processes associated with the UPR and their 45 significantly modulated genes. In addition to the identification of interesting genes associated with the UPR pathway (Fig. S7A-C), target genes of protein kinase R-like ER kinase (PERK) were significantly enriched and upregulated in AccuTOX®-treated groups (GSEA plots in Fig. S7D-E). Overlapping genes, including *Nfyb*, *Exosc7*, *Dis3*, *Exosc2*, *Khsrp*, *Eif2s2*, *Exosc3*, *Exosc8*, *Eif2s1*, *Nfyc*, and *Atf3*, were significantly regulated (adjusted p value < 0.05) in both human and murine models (Fig. S7F). In summary, these analyses revealed that both PERK and IRE1α pathways are prominently modulated in murine and human ARM-X cells in response to AccuTOX® treatment.

Given these observations related to UPR activation in response to AccuTOX® treatment, transcript quantification of each factor related to the three UPR branches was conducted. For instance, treatment of MSCs with the B16F0 lysate admixed with AccuTOX® induces ATF4 expression with no activation observed for this transcription factor if the cells are treated with soluble OVA alone (Fig. 4e—left panel). On the other hand, pulsing of MSCs with AccuTOX® alone or combined with soluble OVA or tumor lysate triggers IRE1α activation, as the ratio of cleaved XBP-1 over unprocessed XBP-1 in response to these three conditions is increased (Fig. 4e—middle panel), whereas none of these treatments activated the ATF6 pathway ((Fig. 4e—right panel). To validate our findings, the ARM-X cells were next tested for their cross-presentation capacity in the presence of pharmacological inhibitors specific to each of these three UPR pathways (Fig. 4f). As expected, treatment with ascending doses of Trazodone (1, 5, 10, 20 μM) resulted in a dose-dependent inhibition in B3Z activation (Fig. 4g), whereas treatment with Salubrinal (5, 10, 25, 50 μM) completely abolished the cross-presentation ability of ARM-X (Fig. 4h). Likewise, inhibiting processing of XBP-1 using KIRA8 (2.5, 5, 10, 20, 40 nM) greatly reduced B3Z activation (Fig. 4i) whereas no change in T-cell activation signal could be observed when AEBSF (75, 150, 300, 600 μM) was used (Fig. 4j). It is worth mentioning that IRE1α/XBP-1 activation in this context does not seem to be dependent on protein aggregation since AccuTOX® mixing with soluble OVA does not lead to the formation of protein aggregates (Fig. S8A) as seen in the context of protein lysate (Fig. S8B) by DLS assessment. These results clearly indicate that the ARM-X cross-presenting capacity relies primarily on the processing of XBP-1 as well as the partial activation of ATF4 in case a tumor lysate preparation is used.

AccuTOX® triggers similar cellular and molecular changes in human ARM-X cells

To ensure that the AccuTOX®-induced properties observed in murine MSCs are clinically translatable, we next investigated whether similar outcomes could be triggered in human BM-derived MSCs. The use of the 10 μM working dose identified in an MTD study (Fig. 5a) effectively enhanced fluorescent OVA uptake (Fig. 5b) and processing (Fig. 5c) while ensuring the retention of an innate MSC phenotype when compared to control human MSCs (Fig. S9). Furthermore, MitoSOX analysis by flow cytometry confirmed ROS induction by AccuTOX® in a time-dependent manner (Fig. 5d). When endosomal escape was investigated, treatment of human MSCs with recombinant Cyt-C admixed with AccuTOX® resulted in apoptosis as shown by Annexin-V staining (Fig. 5e). ROS production in response to AccuTOX® treatment was completely inhibited by NAC treatment in all cases, along with a strong inhibition achieved with α-tocopherol, MitoTEMPO, DPI and ML171 (Fig. 5f). Given the importance of ROS production in UPR induction, we next quantified gene transcription for the three UPR branches in human ARM-X cells. Interestingly, treatment of human ARM-X with both tumor lysate and tumor lysate admixed with AccuTOX® triggers a surge in ATF4 expression, in contrast to soluble OVA, which had no effect on this pathway (Fig. 5g). On the other hand, pulsing with the B16F0 tumor lysate or soluble OVA admixed with AccuTOX® activated XBP-1 processing in both cases (Fig. 5g). As seen in murine ARM-X, these treatments had no impact on the ATF6 pathway (Fig. 5g). Altogether, these data clearly demonstrate that human

ARM-X exhibits enhanced antigen uptake and processing along with ROS production and endosomal escape, akin to the observations made with murine MSCs. In addition, these cells seem to rely on the activation of the IRE1α/XBP-1 axis along with partial activation of ATF4 in response to antigen/AccuTOX® pulsing.

Human MSCs can cross-present antigens in response to antigen/AccuTOX® treatment

Given the lack of an in vitro antigen cross-presentation assay for human MSCs, we next elected to conduct an immunopeptidome study to assess whether human ARM-X can indeed cross-present B16F0 tumor-lysate-derived peptides on cell surface HLA molecules. As human umbilical cord (UC)-derived MSCs may express different HLA levels [59, 60], computational analysis of the immunopeptidome was conducted on both BM- and UC-derived MSCs. Besides the identification of a large set of peptides (595 for BM cells versus 514 for UC cells) that are conserved across all treatment groups, we identified 50 tumor-derived peptides on the surface of BM-derived ARM-X cells (Fig. 6a) versus 19 for UC ARM-X cells (Fig. 6b). Analysis of the peptide motifs for HLA-A2 revealed shared common hydrophobic amino acids at the 2nd and 9th anchor positions for 9-mers long peptides for both BM- (Fig. 6c) and UC-derived ARM-X cells (Fig. 6d) whereas diversified amino acids are detected on positions spanning 3 to 8 for cell preparations (Fig. 6c, d). An analysis ranking these peptides according to their binding affinity demonstrates how most of these sequences bind with high affinity to cell surface HLA molecules on both cell types (Fig. 6e, f). In summary, these data indicate that human BM-derived MSCs can be effectively converted using AccuTOX® to ARM-X cells capable of cross-presenting distinct tumor-derived peptides.

Discussion

Akin to the parent Accum® molecule, the AccuTOX® variant is an injectable anti-cancer molecule [48]. AccuTOX® was found to be non-toxic at the optimal working concentration of 25 μM, and elicited similar effects in murine and human MSCs, underscoring the translational relevance of the work presented herein. Moreover, ARM-X cells are rapidly cleared in vivo, with no sex-biased effects observed. Additionally, no pathological effects were observed beyond minor inflammation at the injection site, and no differential migration patterns of ARM-X cells were observed compared to control MSCs. Once delivered to solid tumors, ARM-X was found to trigger a series of intracellular reactions resulting in excessive ROS production, which in turn causes DNA damage and immunogenic cell death, in line with what was observed for the parent molecule [48].

Interestingly, however, transcriptomic studies revealed yet another characteristic not previously seen with the parent Accum® or A1 molecules. More specifically, AccuTOX® was shown to enhance the process of antigen presentation, an observation that was deemed strategic for the development of a new MSC-based vaccine. When tested on murine MSCs, AccuTOX® was not only well-tolerated, but it enhanced antigen uptake, processing and endosomal release into the cytoplasm. Although these three characteristics are crucial for antigen cross-presentation, the enhanced antigen uptake may explain the salient observation that ~ 10 × less antigen is needed to trigger $CD8^+$ T-cell activation when using AccuTOX compared to the parent molecules. Nevertheless, most of the properties observed with A1 were retained, with the exception of forming protein aggregates, as none could be detected with the use of soluble OVA as shown by DLS analysis. Despite the latter observation, the ARM-X vaccine exhibited signs of UPR activation in both murine and human cells, which begs the question: can UPR activation solely represent a"stem switch"converting culture-adapted immune-suppressive MSCs into potent APCs? Based on our transcriptomic and cell-based analyses, our data clearly highlight an IRE1α/XBP1 role in murine and human ARM-X cells suggesting that this specific UPR pathway may be triggering antigen cross-presentation abilities in MSCs. In support of this hypothesis, a study by García-González et al. reported that proficient

(See figure on next page.)

Fig. 6 Assessment of the cross-presentation capacity of human MSCs using immunopeptidome analysis. **a** UpSet plot showing overlapping and unique peptides in BM-derived human MSCs following B16 lysate pulsing in the presence or absence of AccuTOX®. Set sizes represent the total number of peptides binding to HLA-A*02:01 under each experimental condition, while intersection sizes indicate overlaps. Non-connected dots are unique peptides not shared across conditions. **b** Same as (**a**) but conducted on UC-MSCs. **c** WebLogo showing the sequence motifs of 9-mer peptides derived from B16 lysate admixed with AccuTOX® treatment in BM-MSCs. **d** Same as panel (**c**) but conducted on UC-MSCs. Letter sizes correspond to amino acid frequency, and total letter height reflects information content at each sequence position, measured in bits. **e** Ranking of unique peptides derived from B16 lysate before and after AccuTOX® injection in BM-derived human MSCs. **f** Same as (**e**) but conducted on UC-MSCs. For panels E and F, peptide binding affinities were predicted using NetMHCpan 4.0, where lower values indicate stronger predicted binding affinity

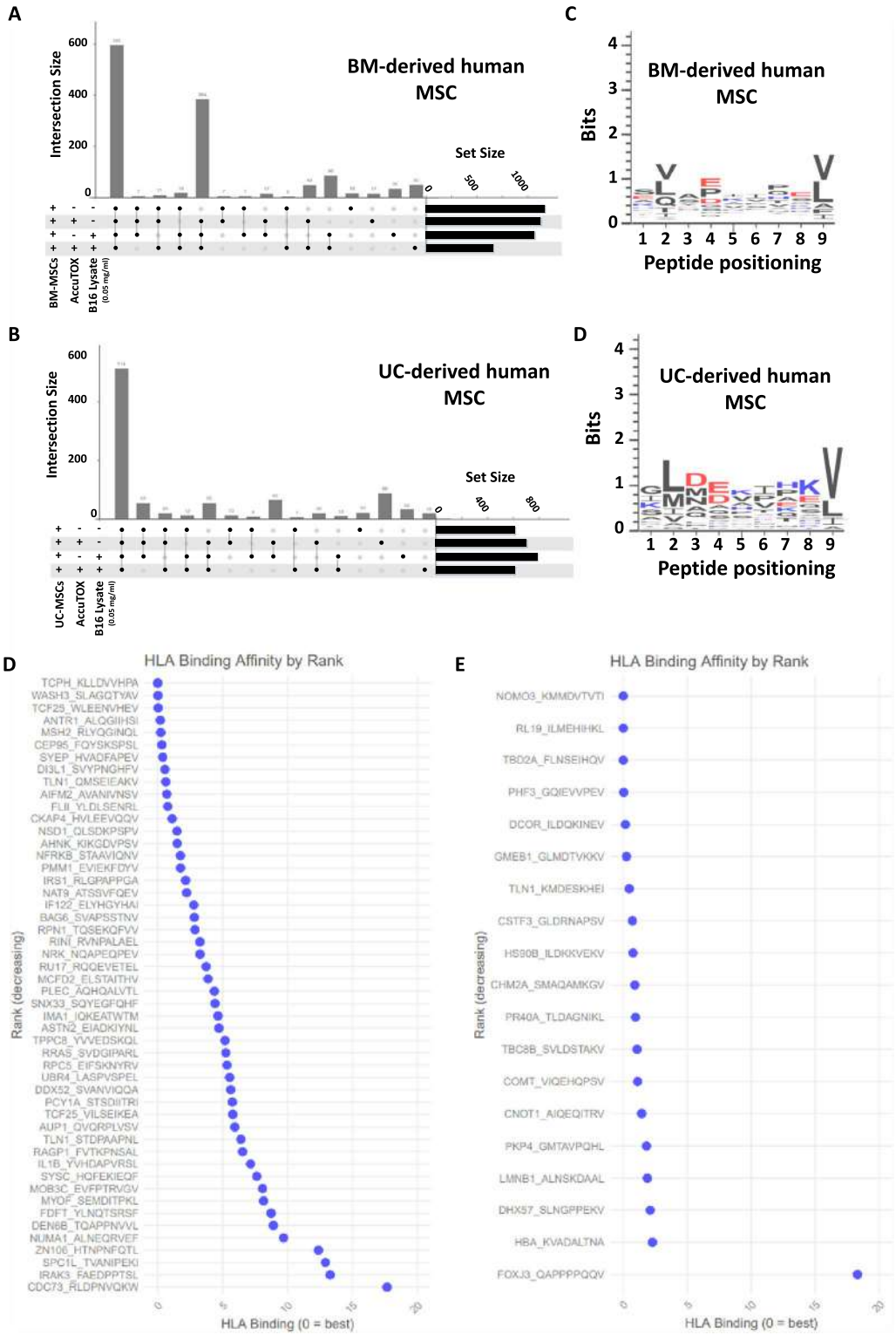

Fig. 6 (See legend on previous page.)

cross-presenting murine $CD8^+$ cDC1 cells show active processing of XBP-1 despite the absence of endoplasmic reticulum stress in these DCs [61]. As such, it would be interesting to investigate whether specific pharmacological activation of the IRE1α/XBP1 pathway directly promotes antigen cross-presentation by MSCs.

Conclusion

In sum, this second-generation ARM-X vaccine is therapeutically superior to the previously tested ARM model, especially when pulsed with low antigen concentrations. The latter property is advantageous as it bypasses a major manufacturing hurdle related to antigen dosing, especially if the vaccine is intended for adaptation to any solid indication. With most of the murine cell observations validated using human BM-derived MSCs, our study demonstrates once more how pharmacological stimulation can drive antigen cross-presentation, with the possibility of testing additional compounds specific to the IRE1α/XBP1 pathway.

Abbreviations

Accum®	Accumulator
ARM	A1-reprogrammed MSCs
ARM-X	AccuTOX®-reprogrammed MSCs
ATF4/6	Activating transcription factor 4/6
APC	Antigen-presenting cell
BM	Bone marrow
CD	Cluster of differentiation
ChAC-NLS	Cholic acid-nuclear localization signal
CTL	Cytotoxic T-lymphocyte
Cyt-C	Cytochrome-C
DC	Dendritic cell
DLS	Dynamic light scattering
DPI	Diphenylleneiodonium chloride
ICI	Immune-checkpoint inhibitor
MTD	Maximum tolerated dose
MHCI	Major histocompatibility complex I
MasdSC	Mesenchymal stromal cell
ML171	2-Acetylphenothiazine
NAC	*N*-Acetyl cysteine
NADPH	Nicotinamide adenine dinucleotide phosphate
NK	Natural killer
OVA	Ovalbumin
PAP	Prostatic acid phosphatase
PD-1	Programmed death 1
PERK	Protein kinase R-like ER kinase
SC	Sub-cutaneous
UC	Umbilical cord
UPR	Unfolded protein response
XBP-1	X-box binding protein 1
WT	Wild-type

Supplementary Information

The online version contains supplementary material available at https://doi.org/10.1186/s13287-025-04465-5.

Additional file 1.

Additional file 2.

Acknowledgements

We would like to thank the staff at the IRIC genomics, proteomics and animal facilities for their kind support regarding the transcriptomics, mass-spectrometry and murine in vivo experiments respectively. Some of the figures shown in the manuscript were generated using the Biorender drawing tool.

Author contributions

JPB conducted most of the in vitro and in vivo studies. NEH worked on all transcriptomics and immunopeptidome-related analyses. GAM, DS, JA, RF, MDG, PM and ML contributed to some in vitro experiments, data analysis and schematic diagram generation. ST contributed to the study design. MR conceived and supervised the project, analyzed all collected data, and wrote the first draft of the manuscript. All authors contributed to manuscript editing.

Funding

The study was funded by a Canadian Institute of Health Research grant (PJT-186233), a research contract research grant provided by Defence Therapeutics Inc. (RB080035) and by a SynergiQC grant from the Consortium Québecois pour le Development de Médicament (RQM00181). GAM is a recipient of a postdoctoral fellowship from the National Sciences and Engineering Research Council of Canada. RF is the recipient of a PhD award from the Cole Foundation.

Data availability

Data sets and material/reagents analyzed and/or used in this study are available upon reasonable request. All transcriptomic data were deposited in the GEO repository with the accession code: GSE287410.

Declarations

Ethics approval and consent to participate

All animals used in the study were housed in a pathogen-free environment at the animal facility of the Institute for Research in Immunology and Cancer (IRIC) and maintained in accordance with the guidelines approved by the Animal Care Committee of Université de Montréal. The ethics protocol entitled Development of new therapies for modulation of the immune system (Protocol #22-065) was approved in September 2024 by the "comité de déontologie de l'experientation animale" of Université de Montréal. RoosterBio confirms that the human bone marrow aspirates used for the production of RoosterBio's research use only RoosterVial™ products as well as RoosterVial™ products produced for further manufacturing under current good manufacturing practices are ethically sourced from consenting donors. RoosterBio sources commercially available in vitro research use only as well as clinical grade human bone marrow aspirate from qualified proprietary vendors. All human bone marrow aspirate collections are from healthy adult consented donors. Collection protocols and the donor-informed consent documents are approved by an Institutional Review Board (IRB).

Consent for publication

Not applicable.

Competing interests

Daniela Stanga and Marina P. Gonçalves were employees of Defence Therapeutics Inc. at the time of the study and declare competing financial interest. All remaining authors declare no competing interests.

Artificial intelligence (AI)

The authors declare that they have not use AI-generated work in this manuscript.

Author details
[1]Department of Microbiology, Infectious Diseases, and Immunology, Université de Montréal, 2900 Edouard-Montpetit, Montreal, QC H3T 1J4, Canada. [2]Sainte-Justine Hospital Research Centre, Montreal, QC, Canada. [3]Research and Development Branch, Defence Therapeutics Inc., Montréal, QC, Canada. [4]Department of Pharmacology and Physiology, Université de Montréal, Montreal, QC, Canada. [5]Molecular Biology Program, Université de Montréal, Montreal, QC, Canada. [6]Department of Biomedical and Molecular Sciences, Queen's University, Kingston, ON, Canada.

Received: 24 January 2025 Accepted: 13 June 2025
Published online: 15 July 2025

References

1. WHO. Cancer. https://www.who.int/news-room/fact-sheets/detail/cancer#:~:text=Key%20facts%201%20Cancer%20is%20a%20leading%20cause,and%20lack%20of%20physical%20activity.%20...%20More%20items
2. Taefehshokr P, et al. Cancer immunotherapy: challenges and limitations. Pathol Res Pract. 2022;229: 153723. https://doi.org/10.1016/j.prp.2021.153723.
3. Lin S-A, et al. Cancer vaccines: the next immunotherapy frontier. Nat Cancer. 2022;3(8):911–26. https://doi.org/10.1038/s43018-022-00418-6.
4. Saxena VDB, Melief B. Therapeutic cancer vaccines. Nat Rev Cancer. 2021;21(6):360–78. https://doi.org/10.1038/s41568-021-00346-0.
5. Fotaki J, et al. Cancer vaccine based on a combination of an infection-enhanced adenoviral vector and pro-inflammatory allogeneic DCs leads to sustained antigen-specific immune responses in three melanoma models. Oncoimmunology. 2018;7(3): e1397250. https://doi.org/10.1080/2162402X.2017.1397250.
6. van der Burg A, Ossendorp VHM. Vaccines for established cancer: overcoming the challenges posed by immune evasion. Nat Rev Cancer. 2016;16(4):219–33. https://doi.org/10.1038/nrc.2016.16.
7. Carreno M, et al. Cancer immunotherapy. A dendritic cell vaccine increases the breadth and diversity of melanoma neoantigen-specific T cells. Science. 2015;348(6236):803–8. https://doi.org/10.1126/science.aaa3828.
8. Palucka B. Cancer immunotherapy via dendritic cells. Nat Rev Cancer. 2012;12(4):265–77. https://doi.org/10.1038/nrc3258.
9. Anassi N. Sipuleucel-T (provenge) injection: the first immunotherapy agent (vaccine) for hormone-refractory prostate cancer. P T. 2011;36(4):197–202.
10. Burch C, et al. Immunotherapy (APC8015, Provenge) targeting prostatic acid phosphatase can induce durable remission of metastatic androgen-independent prostate cancer: a Phase 2 trial. Prostate. 2004;60(3):197–204. https://doi.org/10.1002/pros.20040.
11. FDA. Provenge. Accessed 28–11–2017, https://www.cancer.gov/publications/dictionaries/cancer-drug?CdrID=38038
12. Chen L, et al. Dendritic cell targeted vaccines: recent progresses and challenges. Hum Vaccin Immunother. 2016;12(3):612–22. https://doi.org/10.1080/21645515.2015.1105415.
13. Fu M, Zhou M, Jiang. Dendritic cell-based vaccines against cancer: challenges, advances and future opportunities. Immunol Invest. 2022;51(8):2133–58. https://doi.org/10.1080/08820139.2022.2109486.
14. Bikorimana E-H, et al. Thymoproteasome-expressing mesenchymal stromal cells confer protective anti-tumor immunity via cross-priming of endogenous dendritic cells. Front Immunol. 2020;11: 596303. https://doi.org/10.3389/fimmu.2020.596303.
15. Abusarah K, et al. Engineering immunoproteasome-expressing mesenchymal stromal cells: a potent cellular vaccine for lymphoma and melanoma in mice. Cell Rep Med. 2021;2(12): 100455. https://doi.org/10.1016/j.xcrm.2021.100455.
16. Bikorimana E-H, et al. The CIt protocol: a blueprint to potentiate the immunogenicity of immunoproteasome-reprogrammed mesenchymal stromal cells. iScience. 2022;25(12):105537. https://doi.org/10.1016/j.isci.2022.105537.
17. Goncalves F, et al. A1-reprogrammed mesenchymal stromal cells prime potent antitumoral responses. iScience. 2024;27(3):109248. https://doi.org/10.1016/j.isci.2024.109248.
18. Pelled G, Aslan G. Mesenchymal stem cells for bone gene therapy and tissue engineering. Curr Pharm Des. 2002;8(21):1917–28.
19. Min S, et al. Significant improvement of heart function by cotransplantation of human mesenchymal stem cells and fetal cardiomyocytes in postinfarcted pigs. Ann Thorac Surg. 2002;74(5):1568–75. https://doi.org/10.1016/s0003-4975(02)03952-8.
20. Meirelles Lda N. Murine marrow-derived mesenchymal stem cell: isolation, in vitro expansion, and characterization. Br J Haematol. 2003;123(4):702–11. https://doi.org/10.1046/j.1365-2141.2003.04669.x.
21. Caplan. Adult mesenchymal stem cells for tissue engineering versus regenerative medicine. J Cell Physiol. 2007;213(2):341–7. https://doi.org/10.1002/jcp.21200.
22. Caplan C. The MSC: an injury drugstore. Cell Stem Cell. 2011;9(1):11–5. https://doi.org/10.1016/j.stem.2011.06.008.
23. Le Blanc R, et al. Treatment of severe acute graft-versus-host disease with third party haploidentical mesenchymal stem cells. Lancet. 2004;363(9419):1439–41. https://doi.org/10.1016/s0140-6736(04)16104-7.
24. Lazarus K, et al. Cotransplantation of HLA-identical sibling culture-expanded mesenchymal stem cells and hematopoietic stem cells in hematologic malignancy patients. Biol Blood Marrow Transpl. 2005;11(5):389–98. https://doi.org/10.1016/j.bbmt.2005.02.001.
25. Hahn C, et al. Pre-treatment of mesenchymal stem cells with a combination of growth factors enhances gap junction formation, cytoprotective effect on cardiomyocytes, and therapeutic efficacy for myocardial infarction. J Am Coll Cardiol. 2008;51(9):933–43. https://doi.org/10.1016/j.jacc.2007.11.040.
26. Ren Z, et al. Mesenchymal stem cell-mediated immunosuppression occurs via concerted action of chemokines and nitric oxide. Cell Stem Cell. 2008;2(2):141–50. https://doi.org/10.1016/j.stem.2007.11.014.
27. Krampera C, et al. Role for interferon-gamma in the immunomodulatory activity of human bone marrow mesenchymal stem cells. Stem Cells. 2006;24(2):386–98. https://doi.org/10.1634/stemcells.2005-0008.
28. Chan T, et al. Antigen-presenting property of mesenchymal stem cells occurs during a narrow window at low levels of interferon-γ. Blood. 2006;107(12):4817–24. https://doi.org/10.1182/blood-2006-01-0057.
29. Stagg. Immune regulation by mesenchymal stem cells: two sides to the coin. Tissue Antigens. 2007;69(1):1–9. https://doi.org/10.1111/j.1399-0039.2006.00739.x.
30. François R-M, et al. Mesenchymal stromal cells cross-present soluble exogenous antigens as part of their antigen-presenting cell properties. Blood. 2009;114(13):2632–8. https://doi.org/10.1182/blood-2009-02-207795.
31. Li C, Li Q. Vaccination efficacy with marrow mesenchymal stem cell against cancer was enhanced under simulated microgravity. Biochem Biophys Res Commun. 2017;485(3):606–13. https://doi.org/10.1016/j.bbrc.2017.01.136.
32. Shammaa E-K, Abusarah R. Mesenchymal stem cells beyond regenerative medicine. Front Cell Dev Biol. 2020;8:72. https://doi.org/10.3389/fcell.2020.00072.
33. Salame B, et al. UM171A-induced ROS promote antigen cross-presentation of immunogenic peptides by bone marrow-derived mesenchymal stromal cells. Stem Cell Res Ther. 2022;13(1):16. https://doi.org/10.1186/s13287-021-02693-z.
34. Stagg P, Eliopoulos G. Interferon-gamma-stimulated marrow stromal cells: a new type of nonhematopoietic antigen-presenting cell. Blood. 2006;107(6):2570–7. https://doi.org/10.1182/blood-2005-07-2793.
35. Abusarah. Engineering a novel cell-based vaccine using immunoproteasome-expressing mesenchymal stromal cells. New York: McGill University Libraries; 2020.
36. Zhang W, et al. Mesenchymal stromal cells equipped by IFNα empower T cells with potent anti-tumor immunity. Oncogene. 2022;41(13):1866–81. https://doi.org/10.1038/s41388-022-02201-4.
37. Shi Z, et al. Engineered mesenchymal stem/stromal cells against cancer. Cell Death Dis. 2025;16(1):113. https://doi.org/10.1038/s41419-025-07443-0.
38. Papait S, et al. The multifaceted roles of MSCs in the tumor microenvironment: interactions with immune cells and exploitation for therapy. Front Cell Dev Biol. 2020;8:447. https://doi.org/10.3389/fcell.2020.00447.

39. Minev B, et al. Mesenchymal stem cells—the secret agents of cancer immunotherapy: Promises, challenges, and surprising twists. Oncotarget. 2024;15:793–805. https://doi.org/10.18632/oncotarget.28672.
40. Lacasse B, Jean L. A novel proteomic method reveals NLS tagging of T-DM1 contravenes classical nuclear transport in a model of HER2-positive breast cancer. Mol Ther Methods Clin Dev. 2020;19:99–119. https://doi.org/10.1016/j.omtm.2020.08.016.
41. Bikorimana S, et al. Promoting antigen escape from dendritic cell endosomes potentiates anti-tumoral immunity. Cell Rep Med. 2022;3(3):100534. https://doi.org/10.1016/j.xcrm.2022.100534.
42. Bikorimana A, et al. An engineered Accum-E7 protein-based vaccine with dual anti-cervical cancer activity. Cancer Sci. 2024. https://doi.org/10.1111/cas.16096.
43. Steinman. Dendritic cells and the control of immunity: enhancing the efficiency of antigen presentation. Mt Sinai J Med. 2001;68(3):160–6.
44. Kurts. Cross-presentation: inducing CD8 T cell immunity and tolerance. J Mol Med (Berl). 2000;78(6):326–32. https://doi.org/10.1007/s001090000108.
45. Schaft W, Wohn SD. CD8(+) T-cell priming and boosting: more antigen-presenting DC, or more antigen per DC? Cancer Immunol Immunother. 2013;62(12):1769–80. https://doi.org/10.1007/s00262-013-1481-z.
46. Acosta-Alvear H, Walter A. Homeostasis control in health and disease by the unfolded protein response. Nat Rev Mol Cell Biol. 2024. https://doi.org/10.1038/s41580-024-00794-0.
47. Hetz Z, Kaufman A. Mechanisms, regulation and functions of the unfolded protein response. Nat Rev Mol Cell Biol. 2020;21(8):421–38. https://doi.org/10.1038/s41580-020-0250-z.
48. Bikorimana E-H, et al. Local delivery of accutox(®) synergises with immune-checkpoint inhibitors at disrupting tumor growth. J Transl Med. 2024;22(1):532. https://doi.org/10.1186/s12967-024-05340-2.
49. Eliopoulos F, Boivin MG. Neo-organoid of marrow mesenchymal stromal cells secreting interleukin-12 for breast cancer therapy. Cancer Res. 2008;68(12):4810–8. https://doi.org/10.1158/0008-5472.CAN-08-0160.
50. Dingjan V, et al. Lipid peroxidation causes endosomal antigen release for cross-presentation. Sci Rep. 2016;6:22064. https://doi.org/10.1038/srep22064.
51. Bikorimana E-H, et al. Intratumoral administration of unconjugated Accum impairs the growth of pre-established solid lymphoma tumors. Cancer Sci. 2023;1:234. https://doi.org/10.1111/cas.15985.
52. Nguyen DL. A protocol for macrophage depletion and reconstitution in a mouse model of sepsis. STAR Prot. 2021;2(4):101004. https://doi.org/10.1016/j.xpro.2021.101004.
53. Pang D, et al. Mesenchymal stromal cell apoptosis is required for their therapeutic function. Nat Commun. 2021;12(1):6495. https://doi.org/10.1038/s41467-021-26834-3.
54. Galleu R-V, et al. Apoptosis in mesenchymal stromal cells induces in vivo recipient-mediated immunomodulation. Sci Transl Med. 2017. https://doi.org/10.1126/scitranslmed.aam7828.
55. Giacomini G, Hicks D. The critical role of apoptosis in mesenchymal stromal cell therapeutics and implications in homeostasis and normal tissue repair. Cell Mol Immunol. 2023;20(6):570–82. https://doi.org/10.1038/s41423-023-01018-9.
56. Hetz P. The unfolded protein response and cell fate control. Mol Cell. 2018;69(2):169–81. https://doi.org/10.1016/j.molcel.2017.06.017.
57. Martinotti B, Ranzato A. The unfolded protein response role in cancer. Berlin: Springer; 2019. p. 1–15.
58. Madden L, Healy M, Samali. The role of the unfolded protein response in cancer progression: From oncogenesis to chemoresistance. Biol Cell. 2018;111(1):1–17. https://doi.org/10.1111/boc.201800050.
59. Zoehler F, et al. HLA-G and CD152 expression levels encourage the use of umbilical cord tissue-derived mesenchymal stromal cells as an alternative for immunosuppressive therapy. Cells. 2022. https://doi.org/10.3390/cells11081339.
60. Weiss A, et al. Immune properties of human umbilical cord Wharton's jelly-derived cells. Stem Cells. 2008;26(11):2865–74. https://doi.org/10.1634/stemcells.2007-1028.
61. García-González F, Gutiérrez P-C, Osorio. Human cDC1s display constitutive activation of the UPR sensor IRE1. Eur J Immunol. 2022;52(7):1069–76. https://doi.org/10.1002/eji.202149774.

Publisher's Note